Monitoring and Mapping Floodplain Understorey and Short Vegetation Evapotranspiration

(Progress Report)

Huade Guan, Robin Keegan-Treloar, Wenjie Liu, Karina Gutierrez-Jurado

David Bruce, Robert Keane, Lawrence Burk, Okke Batelaan

National Centre for Groundwater Research and Training, &

Ecology, Evolution and Environment, College of Science and Engineering

Flinders University, Australia

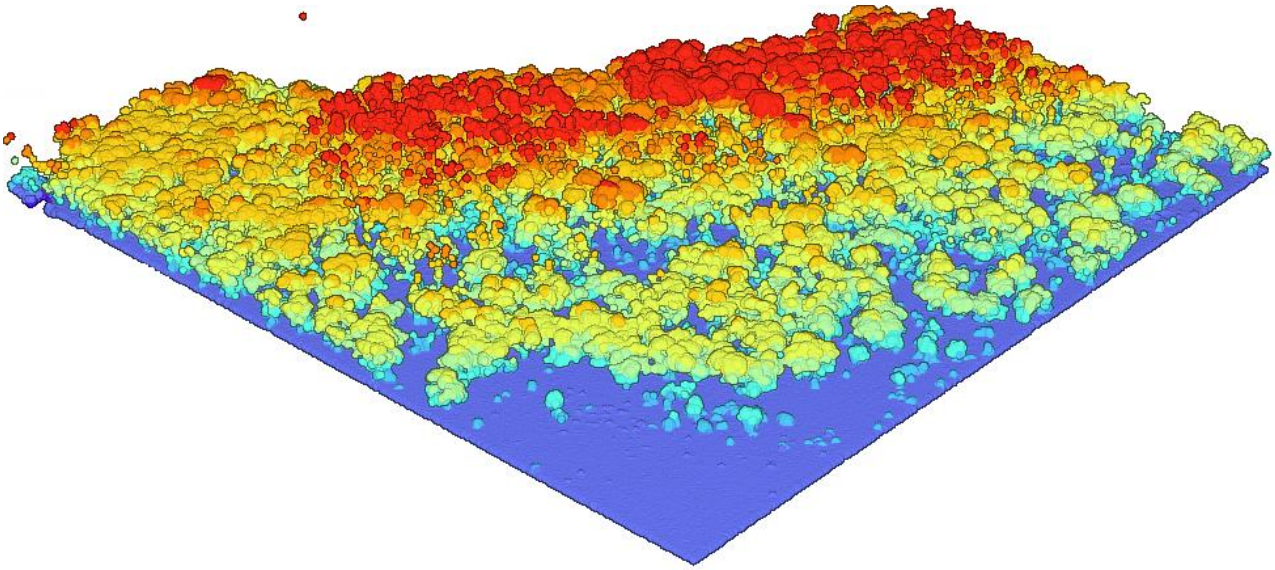

5th July, 2022

Acknowledgement

This ongoing project is funded by Murray-Darling Basin Authority. The idea of using the Maximum Entropy Production (MEP) method for floodplain ET monitoring initiated from earlier discussions for an ARC Linkage proposal, among Flinders University, Murray-Darling Basin Authority (MDBA), CSIRO, and Department of Environment and Water (DEW) South Australia. Juliette Woods (DEW) and Rob Kingham (MDBA) coordinated most of those meetings.

Many people have contributed to this project. Jessica Thompson from MDBA liaised with relevant organsiations for the project and provided support on the project operation. Tanya Doody from CSIRO contributed an MEP station to the project, and her team, Steve Gao and others, provided rainfall observations for the project. Steve Clark provided permission for the project to conduct observations on the floodplain. Jingfeng Wang from Georgia Institute of Technology provided expert support on the MEP method application for the study area. Pao-Yu Huang, Malinee Thongmee-Burk, Zhechen (Oliver) Zhang and Claire Moore from Flinders University assisted with fieldwork.

Abstract

Understorey evapotranspiration (ET) is an important unknown in the water balance of the Murray-Darling Basin. This study adapted a novel method, i.e., Maximum Entropy Production (MEP) ET modelling, for monitoring and mapping ET from floodplain woodland understorey and short vegetation surfaces. The understorey in a River Red Gum woodland and a Black Box woodland are investigated, together with two surfaces covered by Lignum shrubs and Copperburr bushes. The investigation is based on continuous data collection at three stations and about 30 iButton locations, and monthly drone observations, on a Murray River floodplain near Lock 4, Bookpurngong, South Australia.

This progress report summarizes field instrumentation, data collection from spring 2021 to autumn 2022, relevant methods, ET modelling with the MEP-ET models and with the Bowen ratio energy balance method, and MEP-based ET mapping from drone observations.

It is demonstrated that the MEP-Evaporation and MEP-Transpiration models provide more reliable estimates of hourly ET than the Bowen ratio method. The report also domonestrates that a combination of global downwelling shortwave radiation and distributed temperature and humidity measurements can provide a parsimonious approach for monitoring the temporal and spatial variation of evapotranspiration from understorey and short-vegetation surfaces in a floodplain environment.

The results indicate that the River Red Gum understorey on average lost 1.2 mm per day over the observation period (September 2021-March 2022), while the Copperburr surface lost 1.7 mm per day, and the Lignum surface lost 2.0 mm per day. These results imply that the floodplain may lose 2.9 ML of water per hectare in a summer half year, solely due to evapotranspiration from understorey and short vegetation surfaces. This may sum up to a significant component of water balance of the Murray Darling Basin.

The project has developed methodology to map floodplain ET from understorey and short vegetation surfaces. This includes a new metnhod to map understorey surface temperature from drone observations, an adapted method to map understorey net radiation, and a site-specific relationship to map River Red Gum leaf area index. With this methodological development, the study demonstrates the reliability of using the MEP-evaporation model for producing understorey hourly and daily ET maps.

Table of Contents

1. Introduction

Understorey evapotranspiration (ET) is an important unknown in the water balance equation of the Murray-Darling Basin. While tree transpiration has been monitored at a number of floodplain sites, evapotranspiration from the woodland/forest understorey and the area covered by short vegetation is the next unknown to be investigated in the floodplain environment. This project aims to monitor and map ET for woodland understorey and areas with short vegetation cover.

Vegetation cover varies over short distances on flood plains due to spatial variation of soil properties, salinity, topographic relief, and depth to groundwater. In addition to transpiration, soil evaporation can be significant in flood plains. Since salinity influences evaporation and transpiration differently, spatial variability of soil salinity complicates the estimation of flood plain ET. In River Murray flood plains, episodic operations of the salt interception schemes create localised groundwater drawdown, which adds another factor to the complexity of flood plain ET estimation. In such an environment, a reliable and small-footprint method is required to measure spatial variable ET and develop an upscaling method.

The objectives of this project are to (1) adapt and apply a novel ET method (Maximum Entropy Production (MEP) – ET) to monitor understorey, and short vegetation ET in a floodplain environment; (2) develop an ET upscaling approach based on temporally continuous data monitoring at selected locations and spatially continuous drone images at selected time points; (3) estimate daily, monthly, and annual floodplain water loss through understorey and short vegetation surface ET over the study period; and (4) improve our understanding of understorey and short vegetation ET processes.

This progress report summarises the first year of method development, field investigations, drone observations, data analysis, ET modelling and mapping, focusing on showcasing and validating the methodology.

2. Methodology

2.1 Study sites and instrumentation

The study site is located in Clark's floodplain in Bookpurnong along the eastern bank of the River Murray in South Australia. Three MEP monitoring stations and thirty temperature and humidity sensors (iButtons) are distributed over the four main vegetation areas in the floodplain (Figure 1).

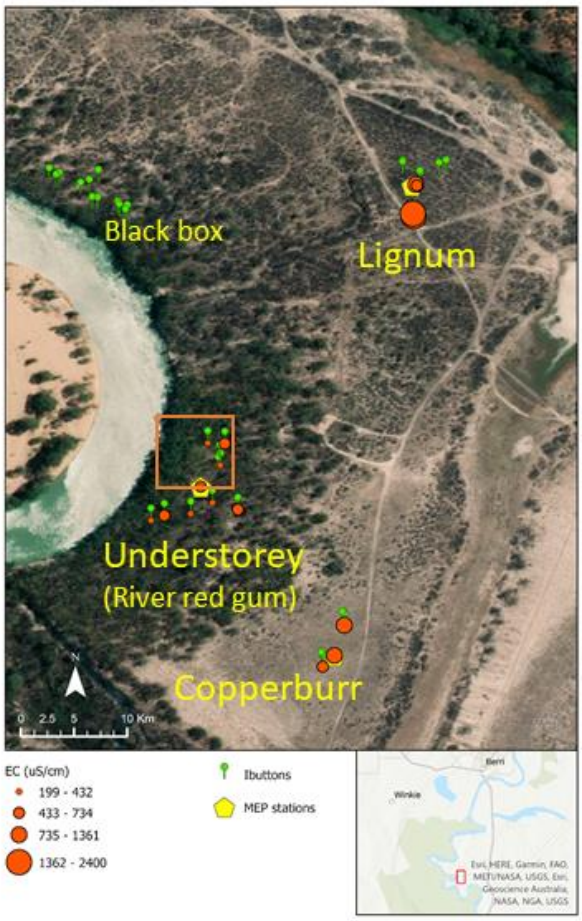

Figure 1 Distribution of field equipment in Clark's floodplain, south of Berri, showing the MEP stations at an understorey River Red Gum woodland, a CCopperburr, and a Lignum site. 30 humidity and temperature sensors are spread over the three sites and a Black Box woodland. Electrical conductivity of the soil surface as a proxy of salinity is shown for the River Red Gum, CCopperburr, and Lignum sites.

The MEP stations for the River Red Gum woodland understorey and the CCopperburr were installed in August 2021 and consist of a net radiometer, a thermal infrared radiometer, and an air temperature and relative humidity sensor. The equipment setup is shown in Figure 2.

Due to a delay in the delivery of new equipment from the provider (Campbell Scientific), the third station at the Lignum site was installed in October 2021. This station is equipped with a four-component net radiometer, a net radiometer, a thermal infrared radiometer, four pairs of air temperature and relative humidity sensors, and two ground heat plates (Figure 3).

The three MEP stations provide half-hourly data of net radiation, relative humidity, and air temperature for MEP-ET models. The thermal infrared radiometer provides additional information on surface temperature and inference of plant water stress conditions where applicable. The four-component net radiometer installed in the Lignum site provides downwelling shortwave radiation for radiation

modelling across the floodplain. Similarly, the additional sets of air temperature and relative humidity provide measurements to apply the Bowen ratio energy balance estimation of ET, which will provide independent ET estimates to check the validity of the MEP-ET models.

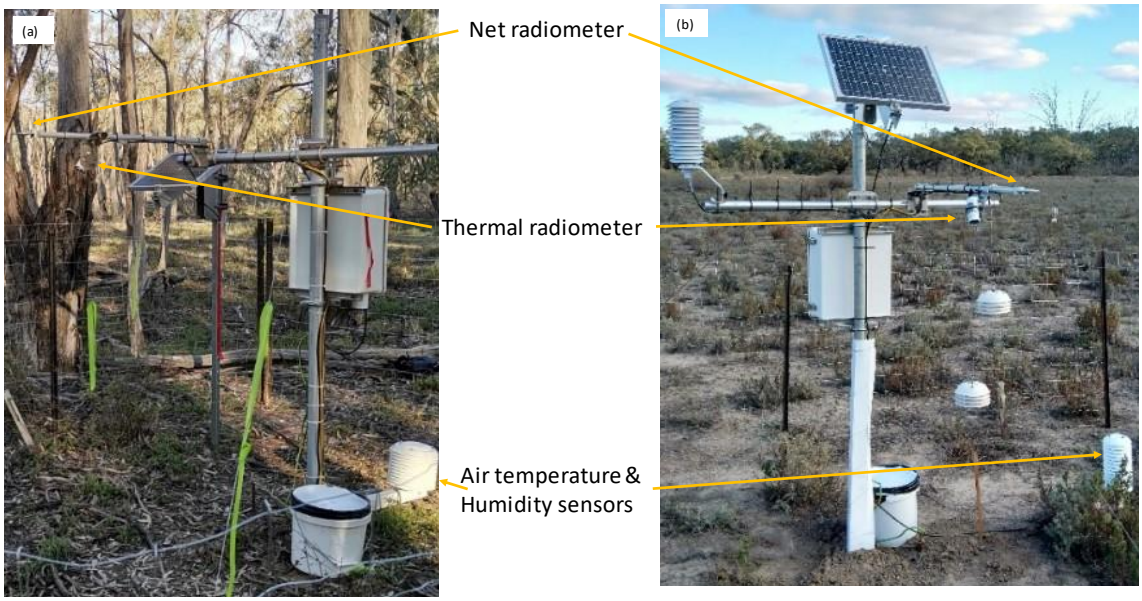

Figure 2 The MEP stations in the a) river red gum woodland understorey and b) at the copper bur site.

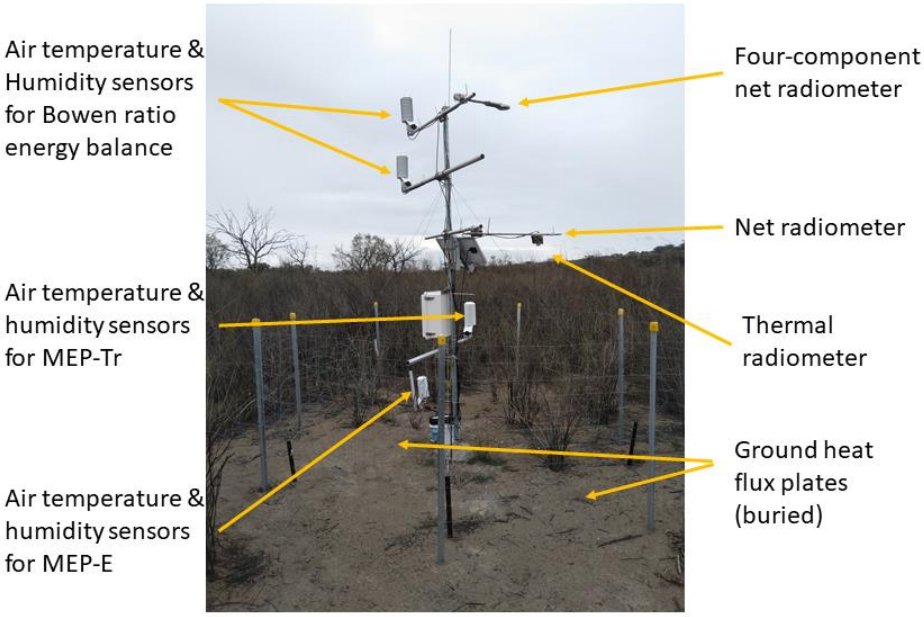

Figure 3 The equipment setup at the Lignum site, including measurements required for MEP modelling of evaporation from the ground and transpiration from the vegetation canopy, and measurements for the Bowen ratio energy balance estimation of ET of the Lignum-covered area.

Figure 4 Photos (from left to right) showing the temperature and humidity sensors installed at (a) the River Red Gum understorey; (b) the Copperburr; and (c)-(d) two levels at the Lignum; and (e)-(f) two levels in the Black Box understorey site.

2.2 Drone Observations

An Unpiloted Aerial Vehicle (UAV) or drone was used to capture thermal infra-red images over three portions of the floodplain representative of the River Red Gum, the Copperburr, and the Lignum areas. LiDAR observations of ground and vegetation height and structure were captured over the whole site. A DJI Matrice 300RTK drone (Figure 5) was used as the flying platform and incorporated a Global Navigation Satellite System (GNSS) receiver and antennae and Inertial Navigation Unit (INU) sensors for position and orientation, respectively.

The thermal infra-red sensor, a DJI Zenmuse H20T 640 sensing 8 -14 µm in a single band, collected images of emitted thermal radiation. Real Time Kinematic (RTK) position and orientation from the drone enabled accurate 3D positioning of each image. Higher spatial resolution images were collected from a 20 megapixel RGB camera simultaneously with the thermal image collection. Differing flight heights were utilised to experiment with joining the thermal images together to create a single temperature mosaic. Whilst lower flight heights above objects (e.g. 40 m) produced smaller pixels, the capacity of automated image matching algorithms to detect unambiguous tie points between images was reduced, particularly over dense tree canopies. Thus, sections such as the River Red Gum site were flown at a larger height above ground level (60 m) to reduce this image matching problem.

Temperature at each pixel was corrected for atmospheric humidity and ambient temperature as recorded by the MET stations. One reason for producing temperature mosaics over small sections of the site was that temperature varied with time. Merging many thermal images together from substantially different times required a time vs temperature correction to be applied. This was further complicated by the fact that automated procedures for generating temperature mosaics chose the best pixel for inclusion of the mosaic based on geometry and radiometry, not on time. The emissivity of sensed objects was assumed to 0.90. This assumption could be refined in future work by predicting the emissivity of every object from image classification. Final temperature mosaics were produced with pixel sizes of 5 cm.

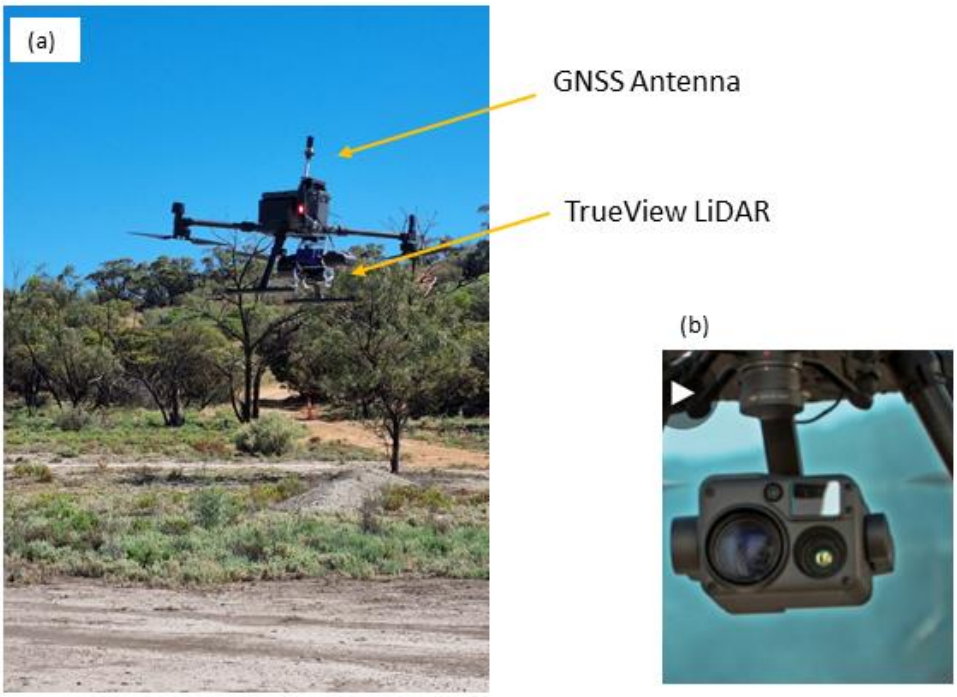

Figure 5 (a) DJI Matrice 300 RTK drone with TrueView 450 LiDAR; (b) Zenmuse H20T Thermal camera.

The 3D observations of ground objects were obtained from a TrueView 450 3DIS LiDAR. This system uses 8 laser beams to produce 430,624 laser pulses per second and records three laser returns per pulse. Simultaneously two 20 megapixel cameras record RGB imagery so that each point in the subsequently generated 3D point cloud can be colorised. The LiDAR sensor has its own GNSS and INU units to record the position and orientation of each laser pulse.

In this case, the LiDAR did not make use of the RTK observations from the Drone. Thus, a GNSS ground station was set up prior to and through the course of LiDAR capture. This ground station recorded the differential GNSS corrections to be applied to the 3D position of every LiDAR pulse and thus involved post-processing of data and enabled actual GNSS satellite orbits to be used, thus improving the quality of the positioning. The LiDAR data was processed in EVO software (a very close relative to LP360) and generated very large 3D point clouds, including positions of ground and above-ground features (grass, shrubs, branches, leaves in trees and canopy surface). The image on the front page of this report shows a perspective view of a 3D point cloud over the River Red Gum site, which has been colorised by height from light green (ground) to dark green (high tree canopy).

2.3 Other sampling and measurements

2.3.1 LAI measurements

Leaf Area Index (LAI) describes the density of canopy cover. It is a dimensionless quantity defined as the green leaf area over the unit ground surface. In this project, we estimate the LAI from light detection and ranging (LiDAR) measurements and calibrate it with site observations using an AccuPAR PAR/LAI ceptometer (Model LP-80).

The LAI estimation is based on the Beer-Lambert law [*Wang and Fang*, 2020]:

$$LAI = -\frac{1}{k}\ln(N_{ground}/N_{total}) \quad (1)$$

where N_{ground} is the number of return LiDAR points from the ground level, N_{total} is the total number of the return LiDAR points, and k is the extinction coefficient. An automatic ground surface classification method is applied to the LiDAR point cloud. The non-ground LiDAR points are classified into low vegetation (1-3 m above ground), middle vegetation (3-10 m above ground) and high vegetation (10-30 m above ground) according to their relative height above the ground.

Field observations of LAI are used to calibrate the LiDAR estimations. The AccuPAR sensor measures the Photosynthetically Active Radiation (PAR) above and under the canopy and calculates the LAI based on the following equation:

$$LAI = \frac{\left[\left(1-\frac{1}{2K}\right)f_b - 1\right]\ln\tau}{A(1-0.47f_b)} \quad (2)$$

where K is the extinction coefficient for the canopy, f_b is the incident beam PAR fraction, τ is the ratio of PAR measured below the canopy to PAR above the canopy. $A = 0.283 + 0.785a - 0.159a^2$ (a is the leaf absorptivity in the PAR band (assumed to be 0.9).

We collected LAI data on 11 May 2022. Due to the unstable sky condition on the day, most measurements in the afternoon were found to be not useful. This report adopted the first set of measurements at the iButton points in the River Red Gum woodland understorey site.

Given that LAI field measurement and LiDAR estimation have different spatial resolutions. The site observation is compared to LiDAR-derived LAI at 1 m, 3 m and 5 m spatial resolutions. We found the LiDAR estimation with 1 m resolution to have the highest correlation as shown in Figure 6.

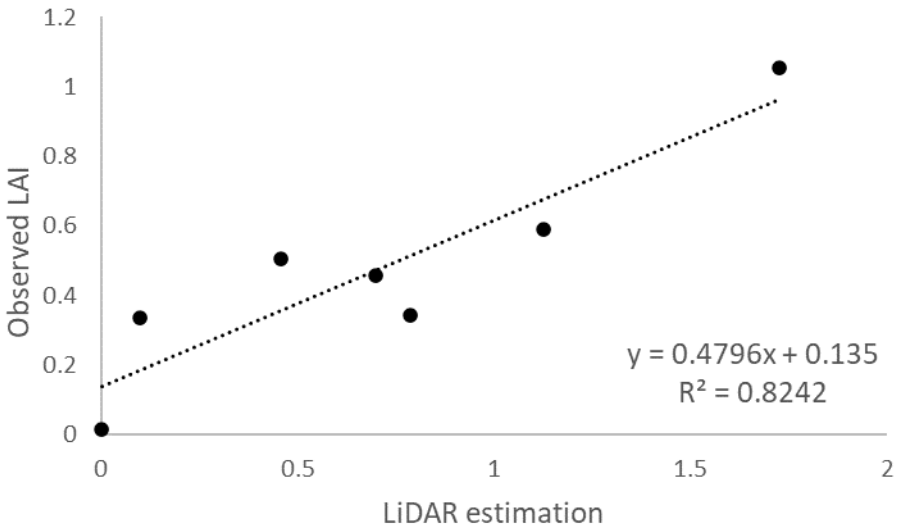

Figure 6 Scatter plot of LiDAR estimated LAI (1 m resolution) versus LAI site observations

2.3.2 Soil salinity measurements

Soil samples were collected at the River Red Gum, the CCopperburr, and the Lignum sites in the first (17-18th August 2021) and second (28th September 2021) equipment installation field trips. The samples

were analysed for soil salinity in the Ecohydrology Research Laboratory at Flinders University. Each soil sample was oven-dried to constant weight at 105 ^{o}C. A mixture of 20 g dry soil sample and 100 ml of deionised water was produced and shaken 100 times. After the sediment was settled, the specific electrical conductivity (EC) was measured in the supernatant using Eutech Oakton COND6+. Altogether, 18 soil EC measurements were obtained, which are presented in Figure 1.

2. 4 The maximum entropy production method

Although the commonly used eddy covariance method can be applied in an understorey environment [*Lamaud et al.*, 2001], it has not been commonly used to monitor understorey ET. This is partly because sensible heat storage in the understorey space and its dynamics increase the complexity of using the method. Another limitation of using the eddy covariance method comes from the size of the homogeneous surface, which is often too small to meet the fetch criteria for the method. The same problems apply to the Bowen ratio energy balance method [*Heilman et al.*, 1989].

Here we apply a new surface energy partitioning method – Maximum Entropy Production [*Wang and Bras*, 2009; *Wang and Bras*, 2011]. The MEP method is different from conventional physically-based methods. It is derived from the maximum entropy theory for the nonequilibrium thermodynamic systems. The MEP method partitions net radiation energy on a surface into sensible heat flux, latent heat fluxes, and ground heat fluxes [*Wang and Bras*, 2011], based on temperature and specific humidity measured at the surface at a regular time intervals (e.g., 30 minute).

The MEP method requires a much smaller set of information than the eddy covariance method, which needs high frequency (e.g., 10 Hz) three-dimensional wind velocity, temperature and specific humidity data. Also, the Bowen ratio energy balance method needs more data; net radiation, ground heat flux, and temperature and humidity at two levels.

Another characteristic of the MEP method is its small footprint of a few meters. Thus, it does not require a fetch as large as 100s of meters as is required for the eddy covariance and Bowen ratio energy balance methods. These characteristics make the MEP method a perfect method to monitor floodplain understorey.

As mentioned above, the MEP method only requires three variables, net radiation (R_n), air temperature (T_a) and specific humidity (q_s) close to the surface from which evaporation or transpiration is to be estimated. The air temperature close to the evaporating surface results from the sensible heat flux, and

humidity is a result of latent heat flux. These measurements are required to construct the "dissipation function" or "entropy production function" [*Wang and Bras*, 2009], which is then solved for the extremum using the Lagrange multiplier method. The mathematical derivation results in the following equations for the MEP-Evaporation model for evaporation simulation (Equations 3, 4, 5) and the MEP-Transpiration model for transpiration simulation (Equations 6 and 7).

$$E + H + G = R_n \tag{3}$$

where *E* is latent heat flux, *H* is sensible heat flux, *G* is ground heat flux.

$$G = \frac{B(\sigma)}{\sigma}\frac{I_S}{I_o}H|H|^{-\frac{1}{6}} \tag{4}$$

where σ is a function of specific humidity and air temperature close to the evaporating surface, I_s and I_o are the inertia terms in defining the entropy production from sensible heat flux and ground heat flux, respectively. $B(\sigma)$is the reciprocal of the Bowen ratio, which can be calculated from σ.

$$E = B(\sigma)\, H \tag{5}$$

$$E_c = \frac{R_n}{1+B^{-1}(\sigma)} \tag{6}$$

where E_c is the transpiration, other symbols were explained earlier.

$$H = \frac{R_n}{1+B(\sigma)} \tag{7}$$

The difference between the MEP-Evaporation and MEP-Transpiration models lies in that the MEP-Evaporation model involves ground heat flux in the energy balance, while the MEP-Transpiration model does not. In this project, we applied MEP-Evaporation for the River Red Gum woodland understorey and the Copperburr surface because the vegetation is within 30 cm of the ground surface. The measured specific humidity near the ground surface (10-30 cm) captures the effect of both soil evaporation and short vegetation transpiration at both sites.

At the Lignum site, we applied MEP-Transpiration to simulate Lignum canopy transpiration and MEP-Evaporation to simulate lignum understorey (mostly bare soil) evaporation. To honour the energy balance in the MEP ET calculation, it is necessary to partition the net radiation between the vegetation

surface and the ground surface. This was done by manually calibrating the ground heat flux estimated with the MEP approach to match the measured ground heat flux by minimising the sum of squared differences. For the final report, we will apply radiation modelling to partition the net radiation as we have done for the River Red Gum woodland site in the report.

The Lignum shrubs are about 1.5 meters high. In this floodplain environment, measurement of air temperature and humidity at this height may be "contaminated" by ambient areas (e.g., nearby river and ponds), which is not representative of the lignum shrubs. Thus, some correction is required [*Gutierrez-Jurado et al.*, 2015; *Hajji et al.*, 2018]. Here we applied a stress factor in the σ function, which is a novel contribution to the method. We adopted a method similar to [*Liu et al.*, 2020], in which air and canopy temperature differences are applied to estimate the water stress for the Lignum MEP-transpiration modelling.

The MEP ET simulations were programmed in Python. The MEP-Evaporation functions were solved iteratively by first setting $H^{(1)} = \frac{R_n}{2}$ then iteratively updating the H estimate using the equation:

$$H^{(k+1)} = \frac{R_n \left|H^k\right|^{\frac{1}{6}}}{\frac{B(\sigma)\, I_s}{\sigma\, I_0} + \left(1 + B(\sigma)\right)\left|H^k\right|^{\frac{1}{6}}} \quad k = 1, 2, 3 \tag{8}$$

We set a convergence criterium of $1E^{-6}$ Wm^{-2} (i.e., the change in *H* values between iterations at which to terminate the model), which was generally met within 6-8 iterations.

2. 5 The Bowen ratio energy balance method

For the Lignum and Copperburr sites, a reasonable fetch is available. We added two levels of air temperature and humidity measurements so that the Bowen ratio energy balance (BREB) method can be applied to produce independent ET estimation concurrent with the MEP ET estimation. At the Lignum site, we also installed two ground heat flux plates. While for the Copperburr site, no ground heat flux was measured, and we used MEP estimated ground heat flux for the BREB method.

The formulation of the BREB method is shown in Equations 9 and 10.

$$E = \frac{R_n - G}{1 + \beta} \tag{9}$$

$$\beta = \gamma \frac{T_1 - T_2}{e_1 - e_2} \quad (10)$$

Where β is the Bowen ratio, T and e are air temperature and vapor pressure measured at two levels vertically, γ is the psychrometric constant.

2. 6 Radiation modelling

To obtain the net radiation of the understorey surface, we simulate the downwelling shortwave radiation and convert the shortwave radiation to net radiation as they are highly correlated [*Jiang et al.*, 2015]. A double-shading transposition (DST) model is employed to estimate the downwelling shortwave radiation for its capacity in simulating the radiation distribution under vegetation cover [*Liu et al.*, 2022]. The model requires the following data: (1) Time and location information; (2) Topography and vegetation data, including digital terrain model (DTM) data, digital surface model (DSM) data, and leaf area index (LAI) data; and (3) Reference radiation data on a horizontal surface, free of shading effects, which shares the same sky condition with the area of interest with solar radiation to be simulated. These data were collected using the methods described in the previous sections. A flowchart for the DST model is shown in Figure 7.

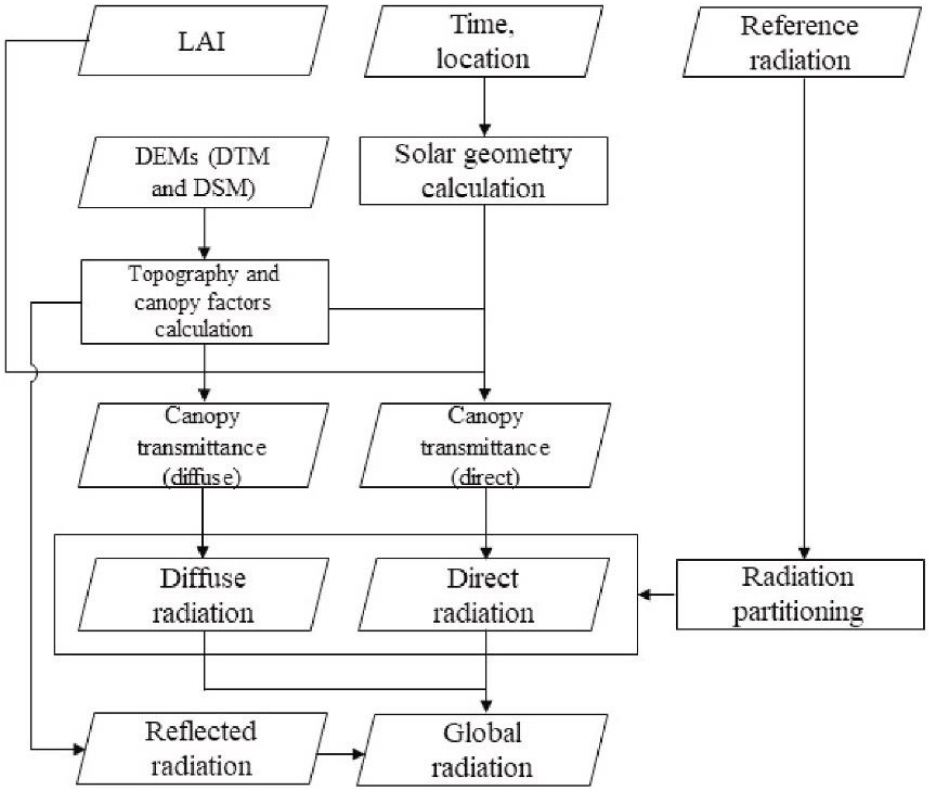

Figure 7 The double-shading transposition (DST) model flowchart.

2. 7 Understorey surface temperature mapping

In addition to the net radiation distribution in the understorey (described in 2.5), the MEP-Evaporation model requires the distribution of surface temperature and specific humidity. The drone observation of surface temperature is a mix of canopy temperatures and understorey surface temperatures. It does not "see" spatially continuous distribution of understorey surface temperatures. Another novel methodology contribution is required in this project to produce the understorey temperature maps.

Firstly, the drone image was categorised into two parts, one for canopy temperatures and the other for the ground temperature. Each covers only part of the total surface area. This separation is based on the LiDAR image. We are then to find the relationship between collocated understorey temperature and LAI. Figure 8 demonstrates this approach.

Regarding the specific humidity mapping, our preliminary exploration of using the Generalised Additive Model shows some promising performance. We will further improve this method, present the result, and incorporate it into the understorey ET mapping in the final report. This progress report uses a simple average of the specific humidity measurements in the River Red Gum understorey site.

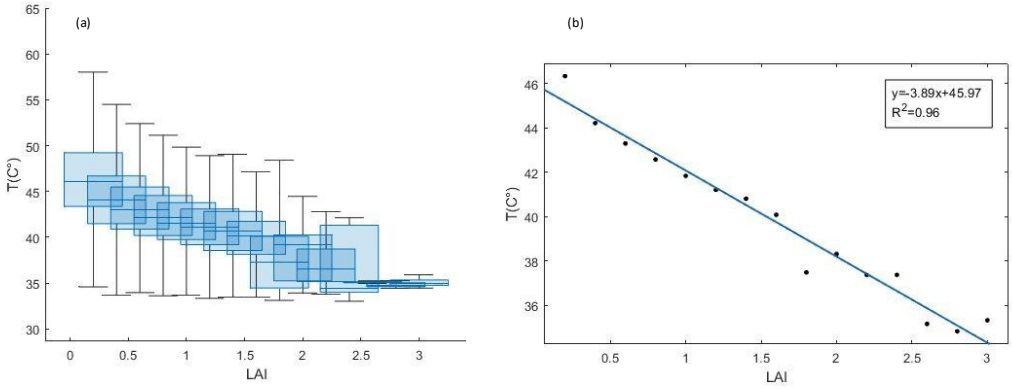

Figure 8 (a) Box plot of ground temperature for each LAI bin; and (b) Linear fitting between the mean values of ground temperature and LAI for individual LAI bins. The temperature data were from the drone measurement around 13:00 on the 4th March 2022.

2.8 Understorey ET mapping

Instantaneous understorey ET mapping will be produced for drone thermal image capture times based on the MEP-Evaporation model. This means that the relevant net radiation mapping and specific humidity mapping should be done for the same time moments.

Once the instantaneous understorey ET maps are produced for all time moments when thermal images are available, they are upscaled to daily ET maps and monthly ET maps based on the diurnal and daily variation of understorey ET patterns from the relevant MEP stations.

We will present these ET mapping products in the final report.

3. Results and Discussion

3.1 Comparison of MEP-ET and the Bowen Ratio Energy Balance method

The validity of the MEP-ET method was assessed by comparing the ET estimates with those obtained using the Bowen Ratio Energy Balance method. This comparison was conducted for both the Copperburr and the Lignum site.

3.1.1 Comparison at the Lignum site

At the Lignum site, temperature and humidity were recorded at two elevations (2.5 and 3 m) along with net radiation of the surface and ground heat flux at 5 cm depth. By adjusting the net radiation to match MEP estimated ground heat fluxes to the observed ones, it yielded a partition of 0.3 whole-surface net radiation to the ground surface and 0.7 to the canopy. Figure 9 displays the observed (x-axis) and calculated (y-axis) ground heat fluxes for the Lignum site with the best fit line in red. As shown, there is good agreement between the observed and modelled ground heat flux from 0-40 W/m^2. However, overestimates the observed ground heat flux for low values (< 0 W/m^2) and underestimates the high ground heat flux values (> 40 W/m^2), as shown by the dots plotting above and below the 1:1 line, respectively.

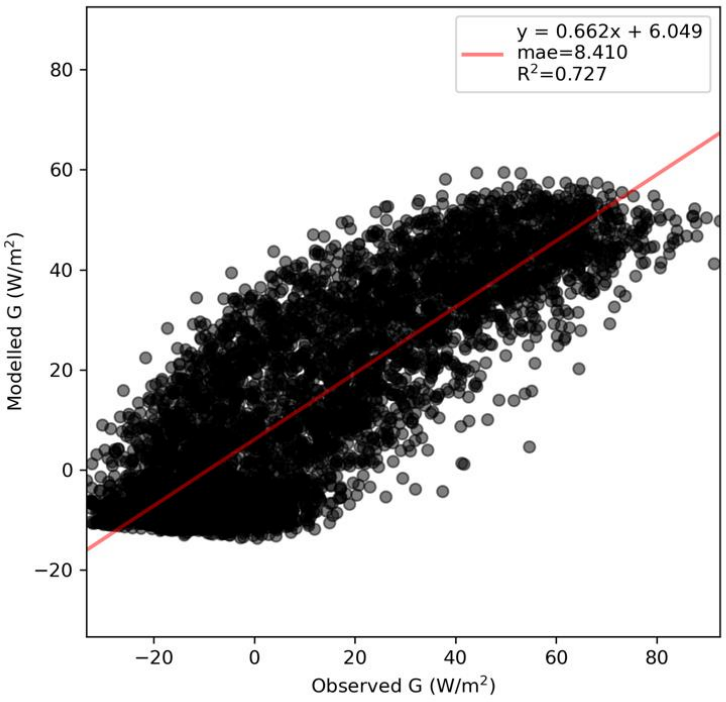

Figure 9 Observed and MEP modelled ground heat flux for the Lignum site with the best fit line shown in red.

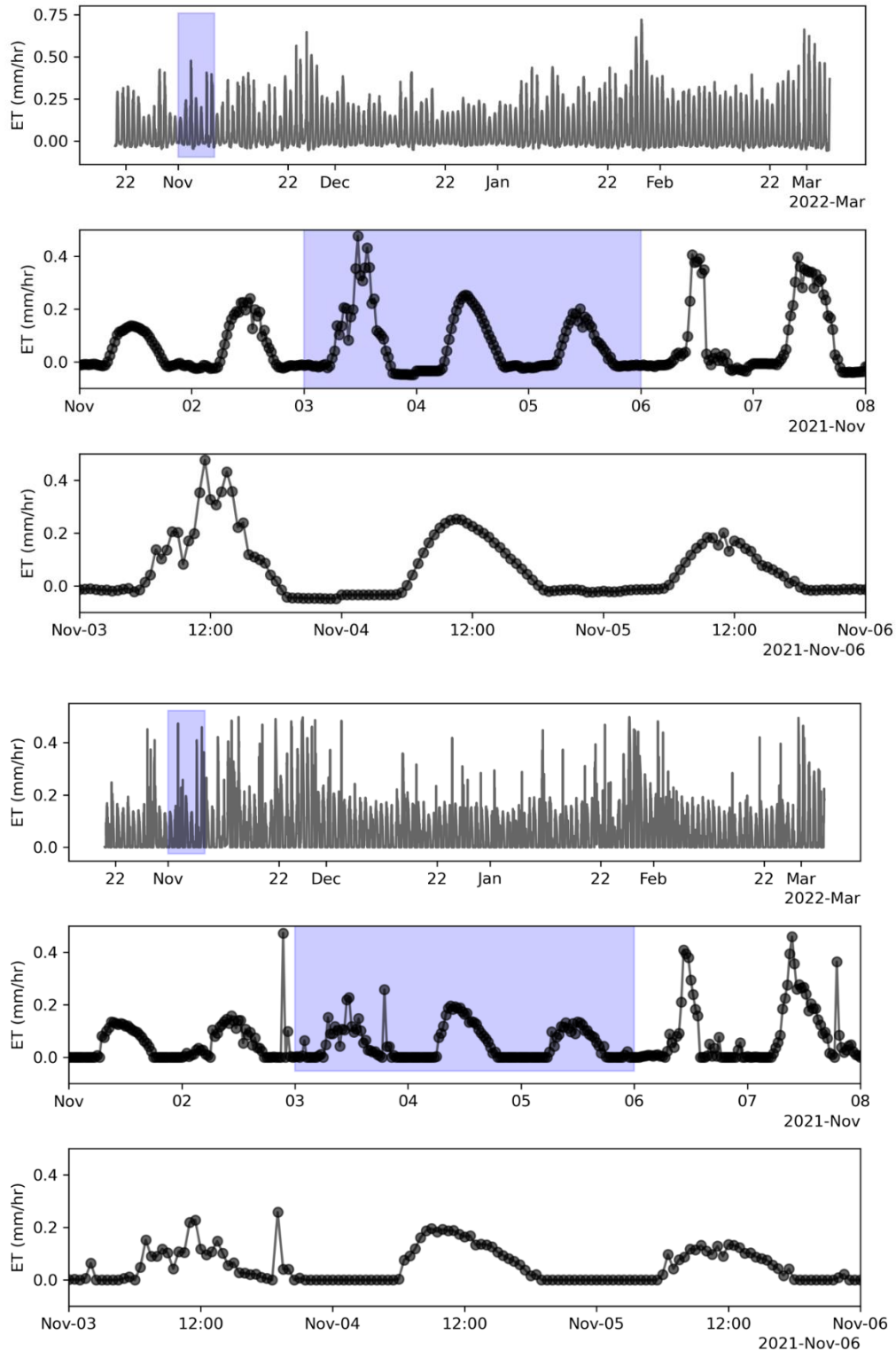

Figure 10 MEP (upper three panels) and BREB (lower three panels) simulated half-hourly ET for the Lignum site. The blue sections show the insets for the relevant zoom-in graphs.

The simulated half-hourly ET are shown in Figure 10 for both MEP and BREB methods. The range of MEP ET is larger than BREB ET. This difference is a reasonable reflection of the different footprint sizes of the two methods (meters for MEP, and tens to hundred meters for BREB). Some spikes in BREB sub-hourly ET do not seem to be physically explainable, which is considered a weakness of the BREB method. In this regard, the MEP method looks more robust. Its sub-hourly ET follows reasonable diurnal cycles.

Figure 11 shows the BREB vs. the MEP daily ET estimates with a blue 1:1 line. The MEP ET estimates are biased towards being larger than the Bowen ratio estimates for the Bowen ratio estimates between 0.5 to 2 mm/day, as shown by the scatter above the 1:1 line. For the larger estimates, the MEP method appears biased towards estimating lower values than the Bowen ratio method, as shown by the scatter below the 1:1 line.

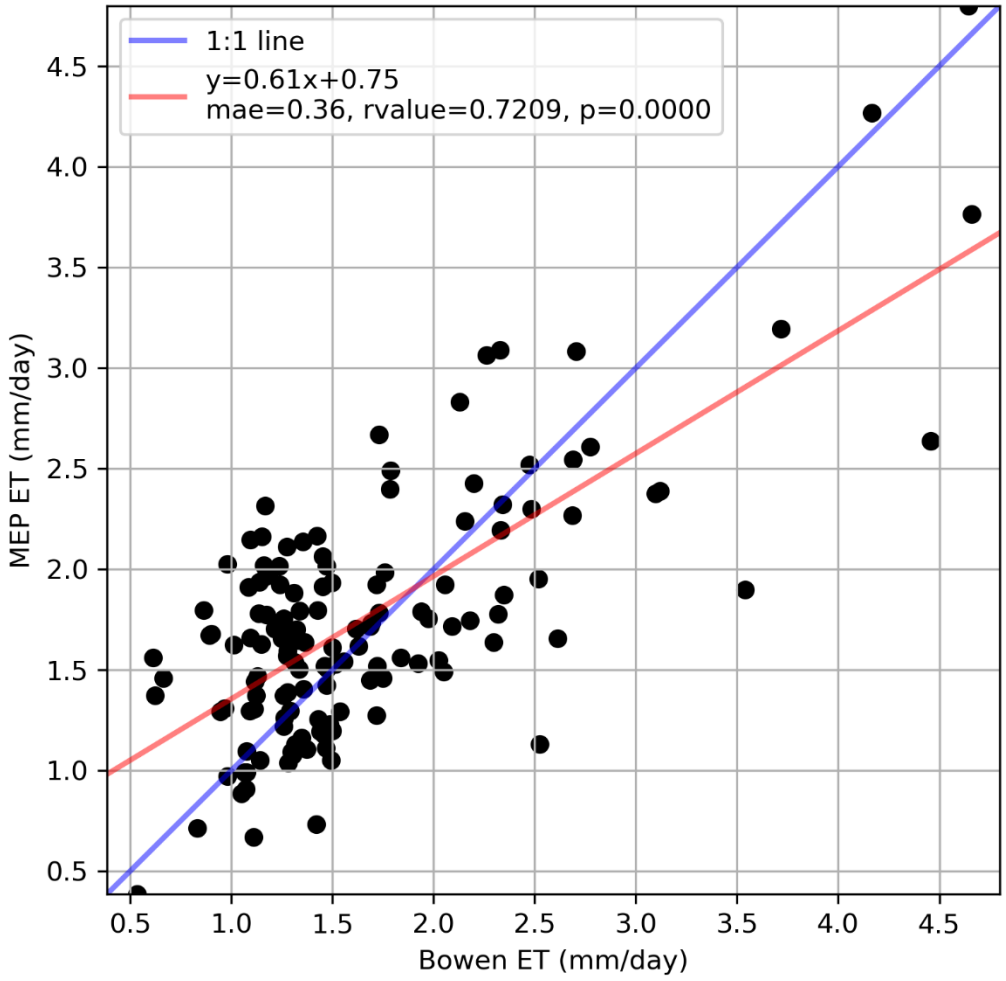

Figure 11 MEP and BREB daily ET estimates for the Lignum site. The blue line is the 1:1 line and the red line is the linear best fit.

This difference may be due to the partitioning of the radiation between canopy and ground surface for the MEP method. If the radiation is partitioned incorrectly, ET estimates may be impacted. Wang and Bras (2011) note that the estimated ground heat flux is typically higher than the measured ground heat flux as the MEP approach estimates at the soil surface, while measurements are typically taken at ~5 cm depth. As the ground heat flux was calibrated to measurements collected at 5 cm depth, our model may underestimate the ground heat flux. As such, an improved approach to radiation partitioning (e.g., radiation modelling) is required to improve the agreement between daily MEP and Bowen ratio ET estimates. We will undertake radiation modelling for the Lignum site. In addition, we will refine the canopy stress function. These improvements will be incorporated into the MEP ET modelling later in the project and included in the final report.

3.1.2 Comparison at the Copperburr site

At the Copperburr site, temperature and humidity were measured at two elevations (0.3 and 1 m), and net radiation was recorded for the site. Unfortunately, ground heat flux was not available. To enable the comparison, the MEP estimated ground heat flux was used as input. In this case, the comparison of the two methods can be viewed on how the two methods partition the available energy (R_n - G).

Figure 12 shows both MEP and BREB estimated half-hourly ET. For the site, the range of sub-hourly ET over the whole period looks similar, probably because the sensors for BREB are within one metre from the ground surface, making the footprint smaller than the Lignum site. The spiky appearance is still there in the BREB estimates. Figure 13 shows the MEP-ET daily estimates in comparison to the Bowen Ratio Energy Balance estimates for the Copperburr site. The relationship follows a linear trend from 0 to 2 mm/day, with estimates from the two approaches being randomly distributed around the 1:1 line. However, from 2 to 3.5 mm/day the MEP-ET method systematically provides lower ET estimates, as shown by the estimates plotting beneath the 1:1 line.

.

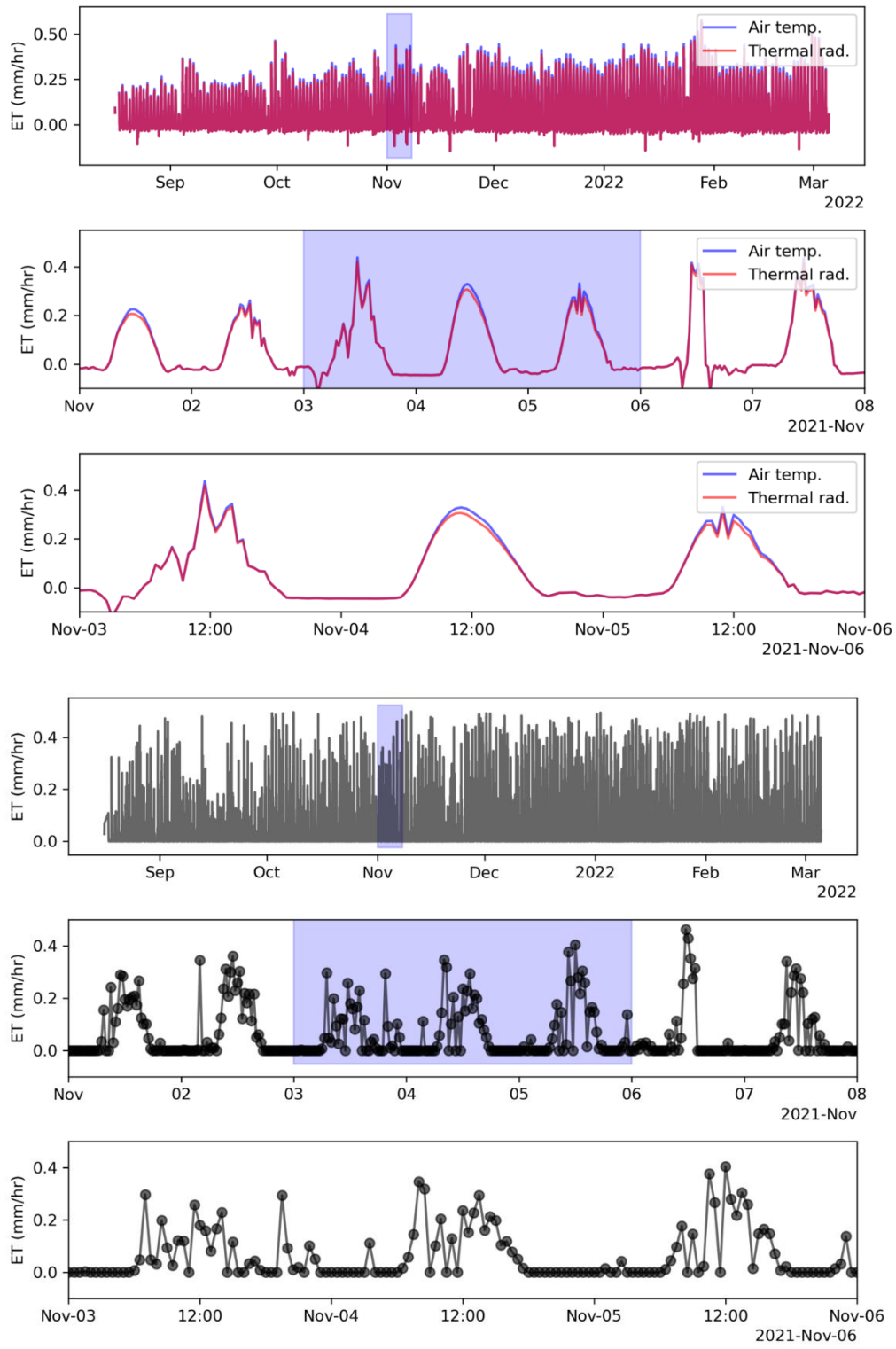

Figure 12 MEP (upper three panels) and BREB (lower three panels) simulated half-hourly ET for the Copperburr site. Two surface temperature measurements (thermal infrared and air temperature were applied for the MEP method. The blue sections show the insets for the relevant zoom-in graphs.

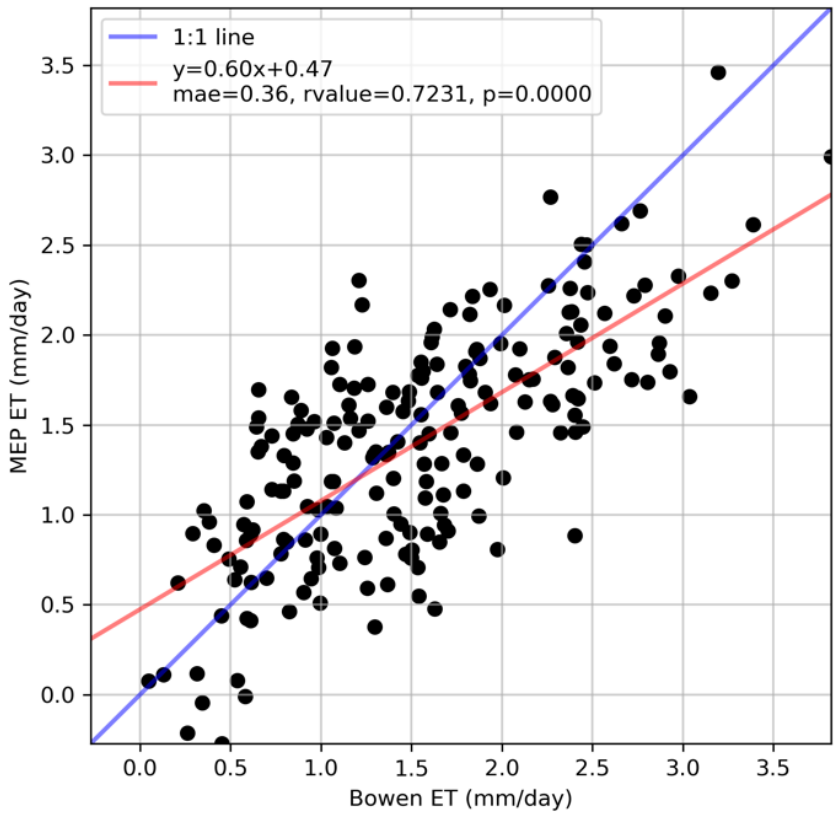

Figure 13 MEP and Bowen Ratio daily ET estimates for the Copperburr site shown with a blue 1:1 line and the linear model of best fit (red line).

The difference may be due to the lower temperature and humidity sensor pairs in the BREB method being too close to the CCopperburr canopy, leading to latent heat overestimation. This notion is consistent with the fact that the bifurcation of the two methods occurs when ET is above 2 mm/day. Another possibility is associated with the instability problem of the BREB method under some conditions. As discussed by [*Payero et al.*, 2003], the Bowen ratio method can become unstable when the Bowen ratio is close to -1, which frequently occurs close to sunrise and sunset. To avoid this problem, Bowen ratio values <-0.75 and >-1.25 were rejected (following Tanner et al. [1987]). However, Payero et al. [2003] note that although this approach is effective at removing most erroneous estimates, some outliers may remain. Erroneous estimates with the Bowen ratio method may be potentially leading to some overly high ET estimates that are not matched by the MEP approach

3.2 ET estimation at the three station locations

Data required for the MEP ET modelling have been collected at the River Red Gum understorey and Copperburr site since August 2021, and at the Lignum site since October 2021. We have simulated ET for three station locations from the start of data collection to April 2022.

3.2.1 ET estimation for the Lignum station

At this site, both MEP-Evaporation and MEP-Transpiration models were applied. For the transpiration model, we adopted the crop water stress index (CWSI) for representing Lignum shrub water stress in calculating the σ function. The CWSI is calculated based on measured canopy temperature and air temperature [*Liu et al.*, 2020]. It has a value between zero and one. A value of one means a complete stress condition under which the vegetation stops transpiration. A value of zero means the vegetation transpires at the potential transpiration rate. Figure 14 shows a time series of daily CWSI for the Lignum site. It tells that a decent size of rainfall can relieve Lignum shrubs' water stress greatly. However, this temporal stress relief does not last more than a week. It also shows that CWSI decreases on some days without observed rainfall. One possibility is that on those days, the atmospheric demand for evaporation is low (e.g., resulting from cloud cover and high humidity), which can relieve plant water stress [*Liu et al.*, 2017; *Yang et al.*, 2013].

Simulated daily ET from both MEP and BREB methods are shown in Figure 15. Over the five months, daily ET varied from 0.5 mm/day to close to 5 mm/day. Averaged over the whole period, the mean daily ET is estimated to be 2.0 mm/day from the MEP method, and 1.7 mm/day from the BREB method. The two estimates are slightly different. We will discuss this difference later in this section.

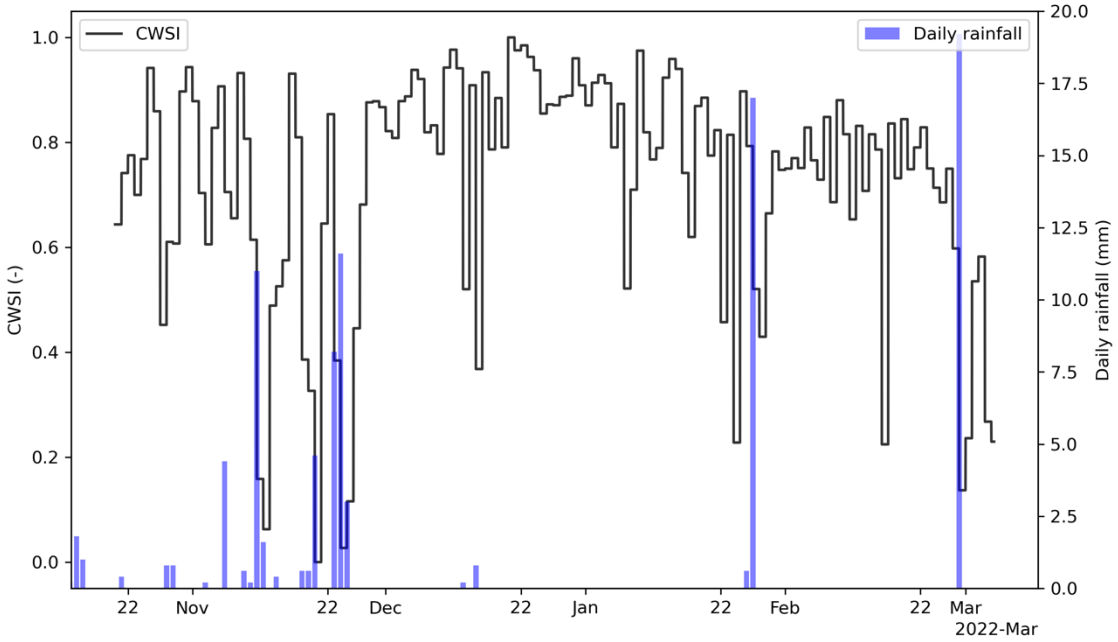

Figure 14 Calculated daily CWSI for the Lignum canopy, together with observed daily rainfall at the site.

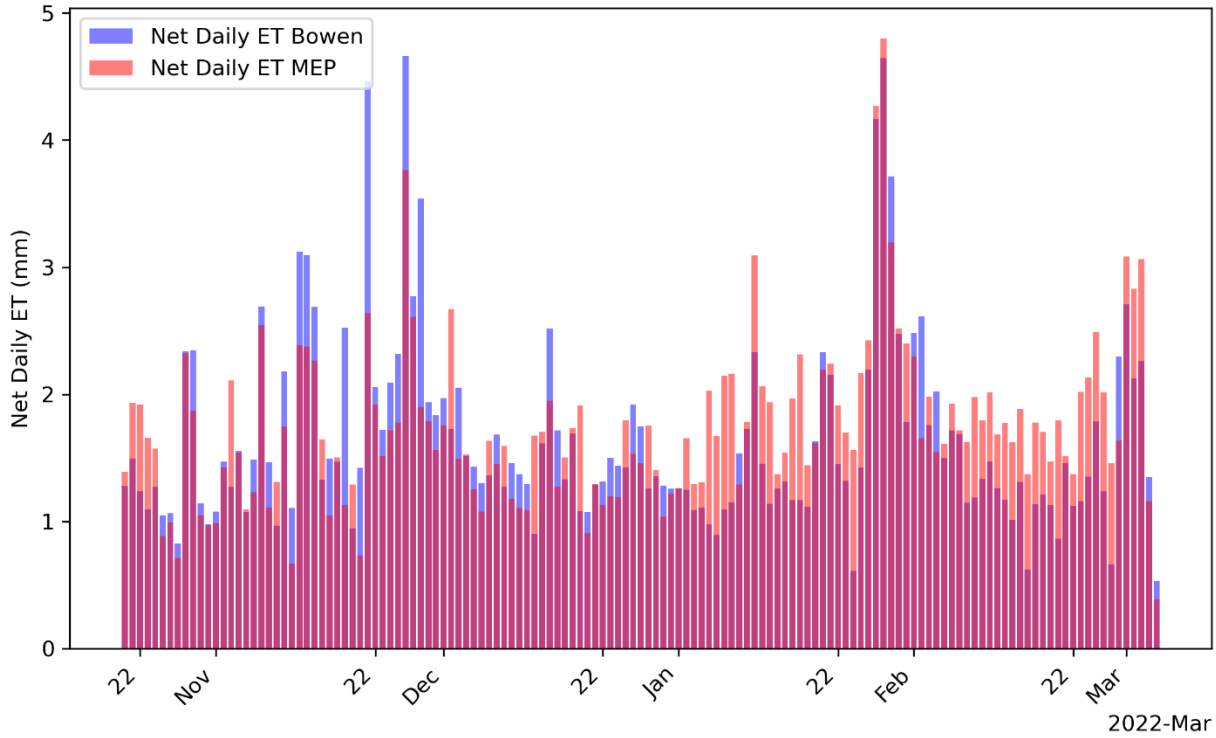

Figure 15 MEP and BREB estimated daily ET from late October 2021 to March 2022 for the Lignum site.

Between estimates from the two methods, MEP more likely estimates larger daily ET than BREB in November and December, while more likely estimates smaller daily ET than BREB in February and March. Although it is not certain from which method(s) the problem comes and what has caused the problem, by comparing the ET estimates among sites, the MEP ET estimates at this site seem to be more consistent with the other two sites (shown later) in terms of the seasonal variation pattern. Thus, the problem is more likely to come from the BREB method. One possibility is that the fetch may vary with season, which impacts the performance of the BREB method. This problem, if correct, is difficult to address. This is the inherent weakness of the BREB method for floodplain ET monitoring.

3.2.2 ET estimation for the Copperburr station

Simulated daily ET for the Copperburr station from both MEP and BREB methods are shown in Figure 15. Over the seven months, daily ET varied from below 0.5 mm/day to around 3.5 mm/day. The mean daily ET over the period was 1.7 mm/day from the MEP method, and 1.9 mm/day from the BREB method. Overall, the MEP method tends to estimate a lower daily ET than the BREB method for this site. As discussed earlier, the lower-level RH/T sensors may be too close to the CCopperburr shrub for the BREB method at this site as these sensors were installed for the MEP method. We will install a new pair of RH/T sensors to check if this is the source of the problem.

Based on the MEP estimates, evapotranspiration at this site was 0.3 mm/day lower than the Lignum site for the whole measurement period.

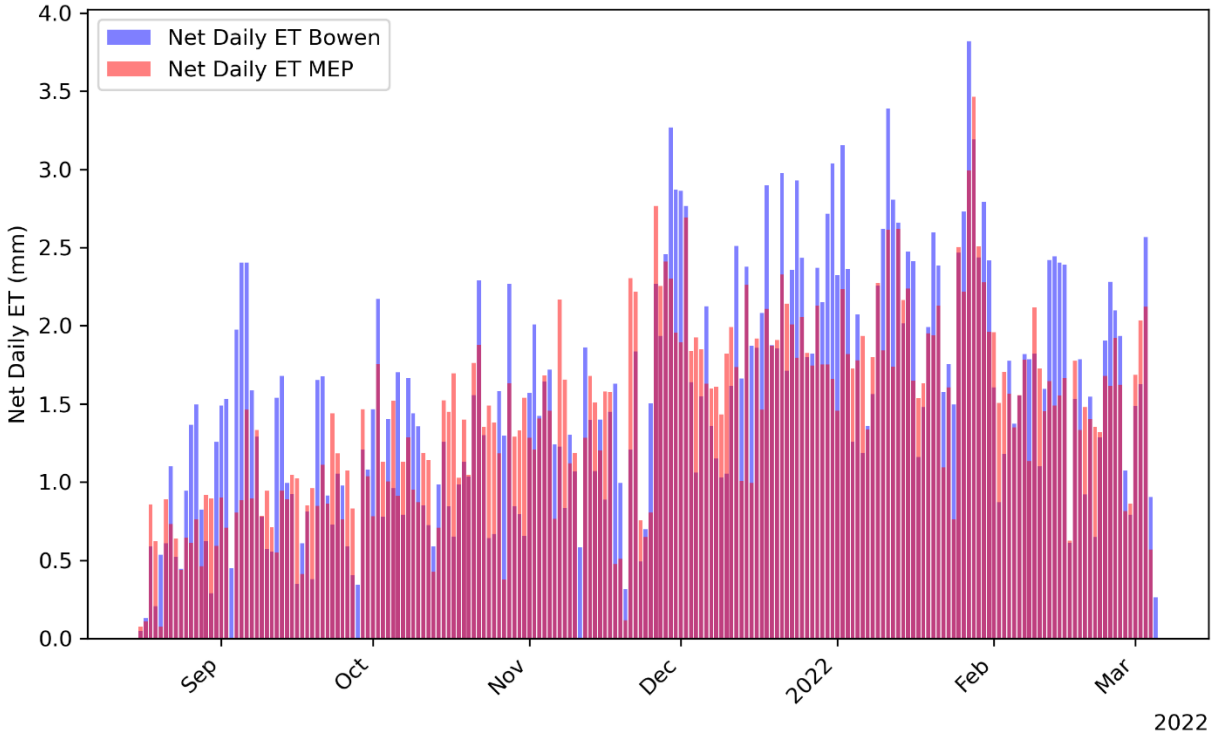

Figure 16 MEP and BREB estimated daily ET from August 2021 to March 2022 for the Copperburr site.

3.2.3 ET estimation for the River Red Gum understorey

For the River Red Gum site, no BREB simulation was available. The MEP simulated half-hourly ET is shown in Figure 17. The temporal variation of ET within a day looks different from the other two sites. This different pattern results from canopy shading induced temporal variation of understorey radiation within a day and thus is a reflection of the reality.

MEP estimated daily ET is shown in Figure 18. The result suggests that the maximum daily ET over the seven months has never exceeded 2.5 mm/day, smaller than the 3.5 mm/day at the Copperburr site, and nearly 5 mm/day at the Lignum site. This is because the radiation input caps the evaporative demand at this understorey environment.

The mean daily ET over the period was 1.2 mm/day. This compares to 2.0 mm/day at the Lignum site, and 1.7 mm/day at the Copperburr site. Using brightness temperature in the MEP-Evaporation model results in a slightly larger estimate of ET than using air temperature measurement. This difference is consistent with our understanding of the method, and the difference is very small.

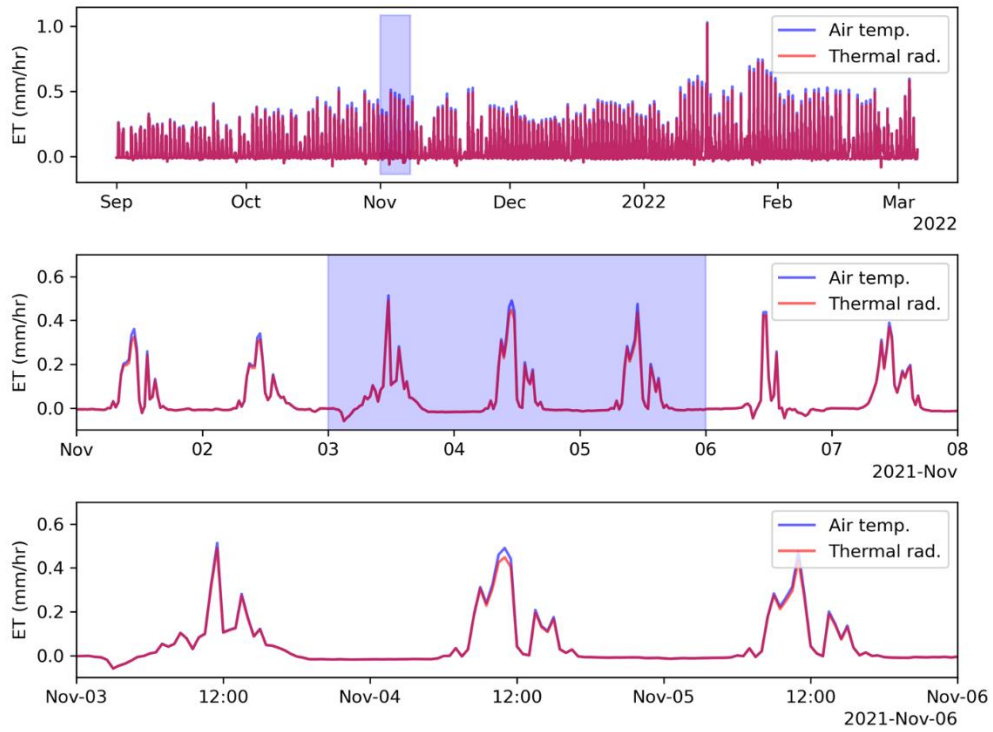

Figure 17 MEP estimated half-hourly ET for the River Red Gum understorey at the station. Two surface temperature measurements were used, leading to a minor difference in the ET estimation.

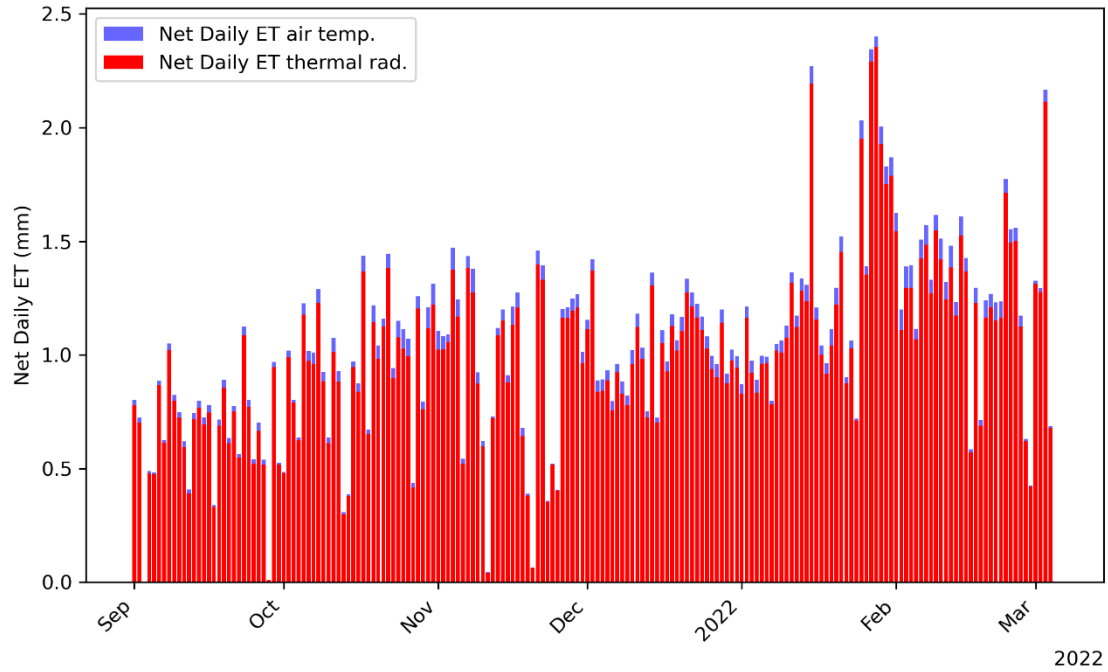

Figure 18 MEP estimated daily ET from September 2021 to early March 2022, using two different surface temperature measurements.

3.3 MEP-ET estimation at the iButton locations

ET was estimated at 16 iButton locations (see photos in Figure 19) at the Copperburr and River Red Gum sites using the modelled radiation and the temperature and humidity measured at each iButton. It was not possible to complete the analysis for the Lignum or Black Box sites as the radiation modelling had not been completed at the time of writing. As shown in Figure 4, there was variability in the vegetation cover measured at each site. For example, at the Copperburr site iButtons 36 and 38 (previously 17 and 18) were located at 15 cm above the Copperburr vegetation, while 35 and 37 were located over bare ground. Similarly, for the River Red Gum site, iButtons 7 and 8 were over moss, iButton 4 over small vegetation and iButtons 5, 6, 9 and 10 on or near spiky bush and iButton 11 was over bare ground. This variability was intentional to allow for the comparison of ET between bare soil and the different vegetation types.

Table 1 provides the monthly average daily ET for each iButton in the study sites. For the River Red Gum site the ET ranges from 0.74 mm/day in November at iButton 4 to 2.23 mm/day in March at iButton 8. Generally, the ET estimates appear to increase from November to February or March, then decrease at a similar rate. This is likely to do with the available radiation (i.e., more daylight in the summer months) and the occurrence of rainfall events. ET over the moss vegetation is highest with iButtons 7 and 8 ranging from 1.6 mm/day in November and May to 2.23 md/day in March. For the bare soil, ET for iButton 11 is lower than ET estimates of all other iButtons (except 6 and 4), with estimates ranging from 1.15 mm/day in December to 1.65 mm/day in April. ET for the spiky bush (iButtons 5, 9 and 10) was greater than the bare ground but less than the moss, with ET estimates ranging from 1.19 mm/day in May to 1.94 mm/day in March. iButtons 4 and 6 had substantially lower ET estimates than the other sites despite being located over vegetation. This was due to shading at these sites, which meant the available radiation likely constrained ET. Overaged over all locations and months, the understorey ET loss is estimated to be 1.5 mm. This number is slightly larger than 1.2 mm estimated based on the MEP station. This difference can be explained by that the two estimates are based on data from different periods: from November to May for iButton locations, and from August to March for the understorey MEP station.

For the Copperburr site, ET ranges from 0.67 mm/day in September 2021 at iButton 17 to a maximum of 2.03 mm/day in February 2022 at iButton 38. As shown, the ET appears to increase from September (~0.67-0.68 mm/day) till February (~2-2.03 mm/day), then decrease at a similar rate till April (~1.28

mm/day). Interestingly, the ET is consistent between iButtons at the Copperbur site and there is minimal difference between the ET in areas of vegetation (iButtons 17, 18, 36 and 38) and non-vegetated areas (iButtons 35 and 37). An average over all locations and months gives 1.6 mm/day. This is close to 1.7 mm/day from the MEP estimate based on the Copperburr station.

Figure 19 Photographs of the installed iButton sensors at the River Red Gum and Copperburr sites. Note iButtons 36 and 38 replaced 17 and 18 following sensor failure.

Table 1 Monthly average daily ET for each iButton at each site. Sensors 17 and 18 failed and were replaced by 36 and 38.

iButton ID	Site	Monthly averaged daily ET (mm/day)								
		Sep 21	Oct 21	Nov 21	Dec 21	Jan 22	Feb 22	Mar 22	Apr 22	May 22
4	River Red Gum			0.74	0.81	0.96	1.15	1.03	0.97	0.74
5	River Red Gum			1.48	1.50	1.43	1.85	1.94	1.77	1.32
6	River Red Gum			1.20	1.13	1.18	1.48	1.48	1.41	1.02
7	River Red Gum			1.60	1.67	1.56	2.08	2.19	2.11	1.60
8	River Red Gum			1.65	1.66	1.58	2.12	2.23	2.15	1.65
9	River Red Gum			1.42	1.31	1.31	1.64	1.61	1.59	1.26
10	River Red Gum			1.42	1.41	1.40	1.81	1.88	1.67	1.19
11	River Red Gum			1.20	1.15	1.21	1.55	1.62	1.65	1.23
12	River Red Gum			1.49	1.43	1.41	1.79	1.83	1.68	1.22
13	River Red Gum			1.42	1.42	1.59	1.83	1.64	1.26	0.89
17*	Copperburr	0.67	0.93							
18*	Copperburr	0.68	0.93							
35	Copperburr			1.29	1.48	1.88	2.02	1.59	1.28	
36 (17)	Copperburr			1.28	1.48	1.87	2.00	1.57	1.28	
37	Copperburr			1.32	1.49	1.88	2.02	1.59	1.28	
38 (18)	Copperburr			1.31	1.50	1.90	2.03	1.41		

3.4 Preliminary LAI, understorey radiation and temperature mapping

Spatially distributed LAI data is required for modelling shortwave radiation, which penetrates into the understorey, and for modelling understorey surface temperature distribution. Based on the LiDAR data and in situ LAI measurements for the iButton sites, a map of LAI was produced and shown in Figure 20. A preliminary test has found that the DST modelling based on this LAI map produces a more reasonable shortwave radiation time series at the understorey station site than that based on the LAI estimates from the NDVI data (image from PlanetScope Dove satellites).

At this stage, a relationship was established between the observed net radiation and DST simulated understorey shortwave radiation for each month. This relationship was then applied to produce understorey net radiation maps. An example map of net radiation distribution is shown for 13:00 (local standard time), 04 March 2022 (Figure 21). A big range of understorey net radiation is seen from the map, suggesting the degree of spatial variability of energy for sensible and latent heat fluxes in the understorey environment. We will refine this method for the final report.

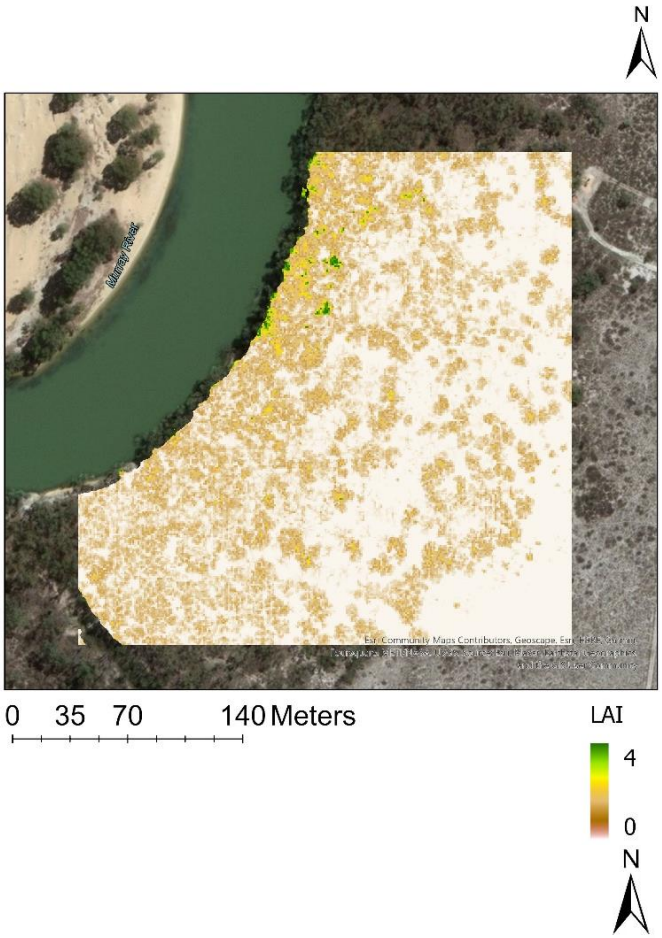

Figure 20 Leaf area index map generated from the LiDAR data calibrated with point LAI measurements for the River Red Gum woodland.

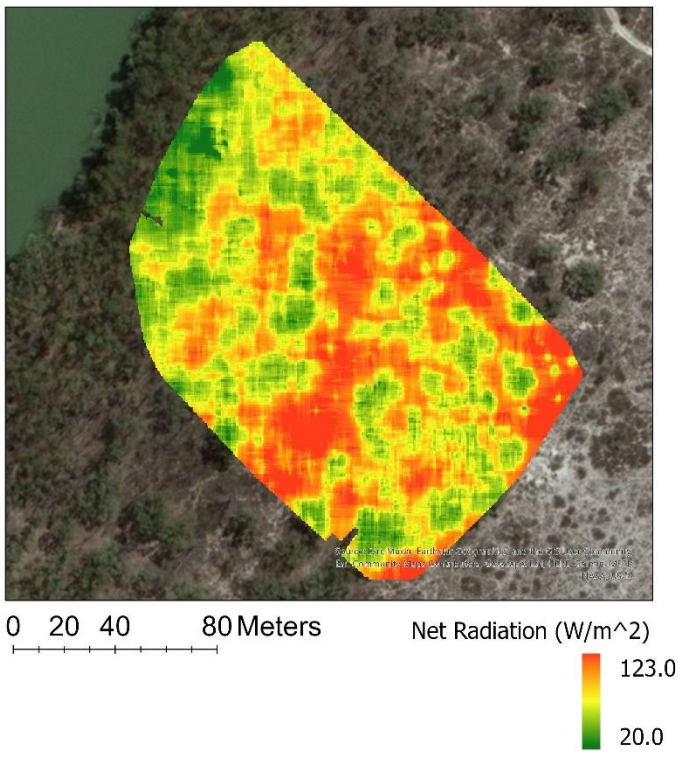

Figure 21 Simulated understorey net radiation on Mar 04, 2022, 13:00

An example of an understorey surface temperature map is shown in Figure 22 for the same time as the net radiation map.

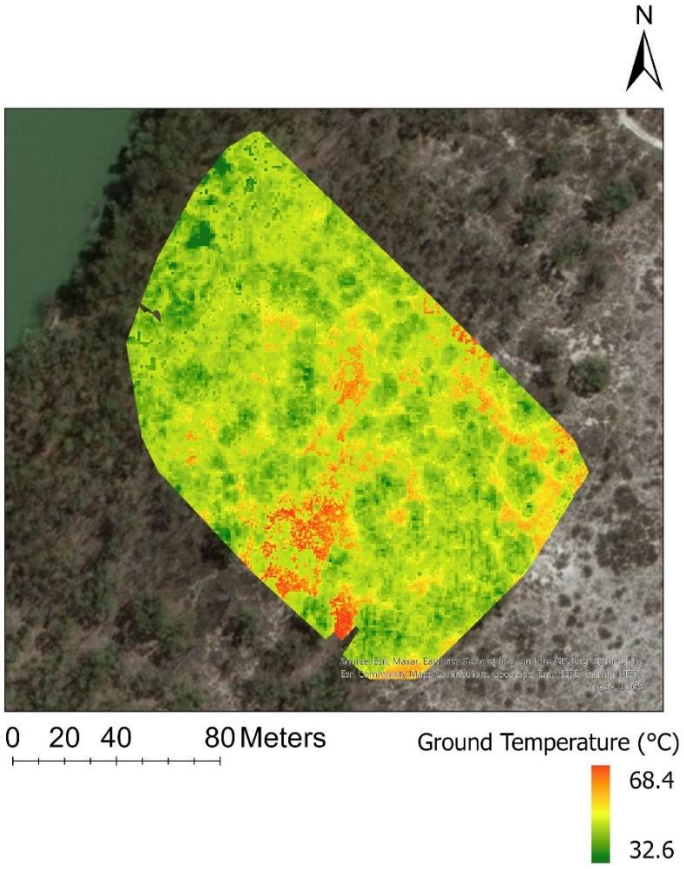

Figure 22 Simulated ground temperature on Mar 04, 2022, 13:00

3.5 Preliminary drone image-based understorey ET mapping

ET was estimated using the temperature and radiation maps and the average q_s for the iButton sites from 12:30-13:00. ET estimates from the mapping inputs were compared with those based on the iButton measuremnets (Figure 23). Figure 24 shows the spatially distributed hourly understorey ET map for the River Red Gum site. This was upscaled to daily estimates by dividing the average hourly ET at the iButton sites by the total daily ET and taking an average to develop a scaling factor. The hourly ET was multiplied by the scaling factor to develop a daily ET map for the site shown in Figure 25.

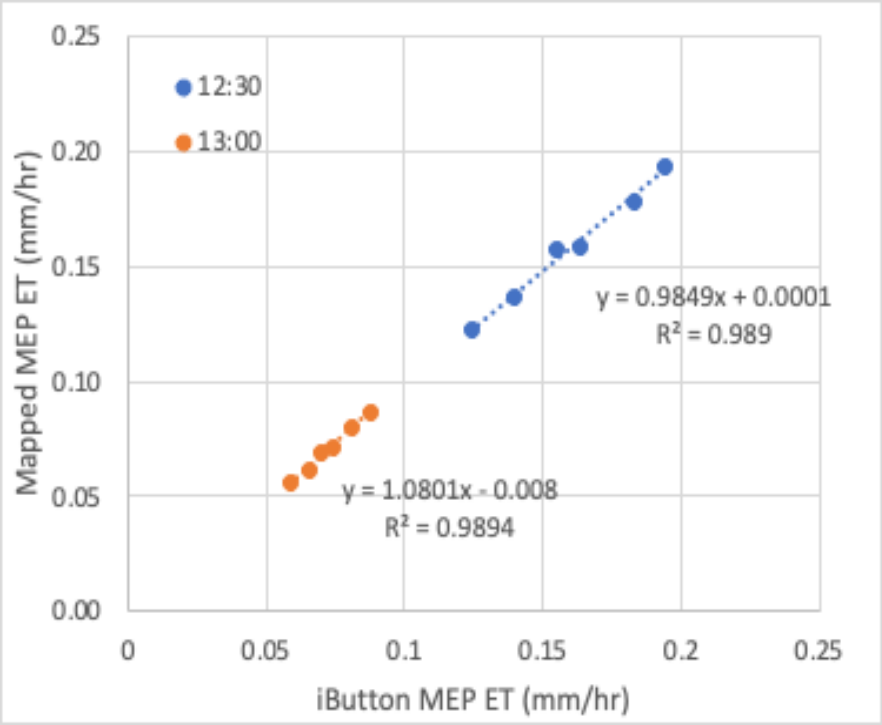

Figure 23 Modelled spatially distributed ET (y-axis) and iButton MEP ET (x-axis) for the raw mapped values (blue dots) and the calibrated mapped values (orange dots).

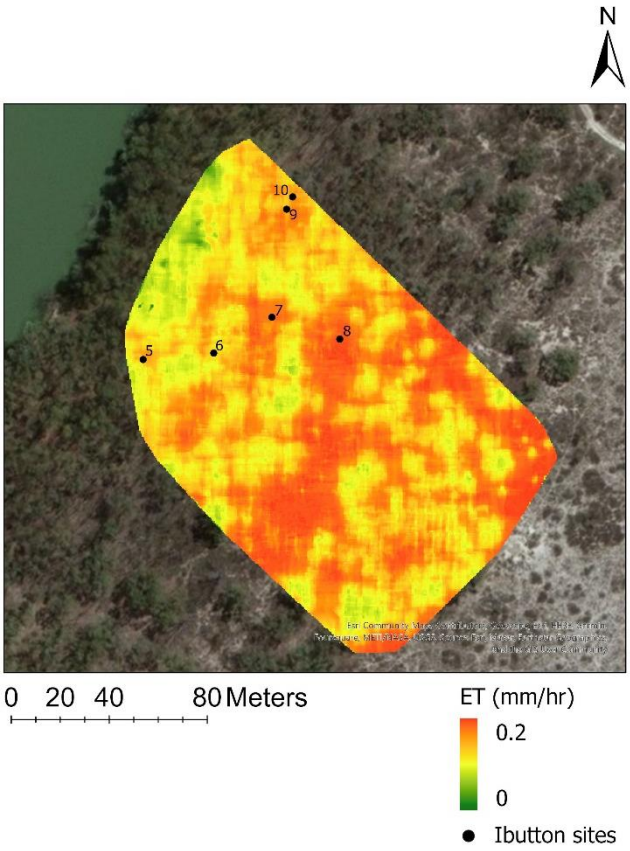

Figure 24 Spatially distributed hourly ET estimated for the time period 12:30 (LST)

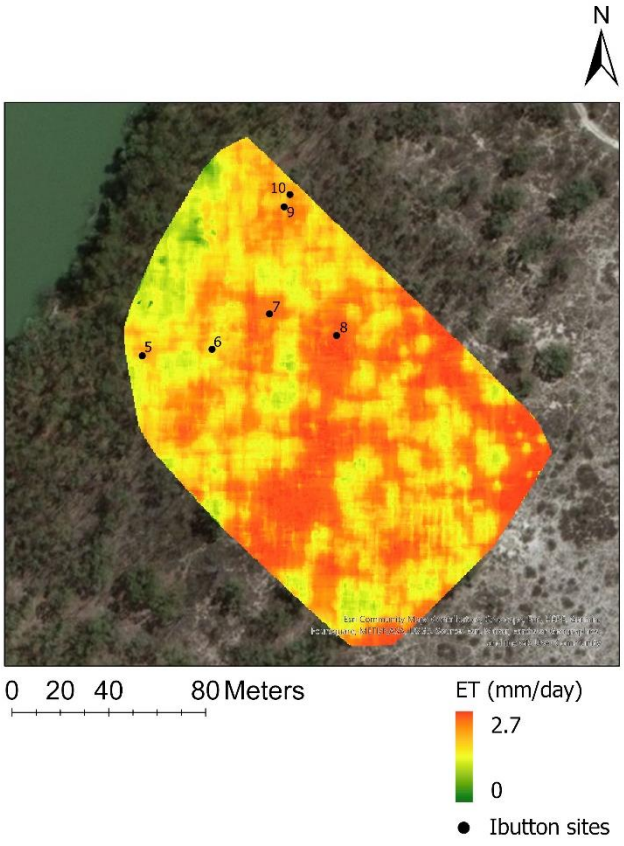

Figure 25 Spatially distributed daily ET for the 4/3/2022 upscaled hourly values in Figure 24.

4. Conclusions

This report summarizes field instrumentation, data collection from spring 2021 to autumn 2022, the relevant adopted and developed methods, ET modelling with the MEP-ET models and with the Bowen ratio energy balance method, and MEP-based ET mapping from drone observations.

It is demonstrated that the MEP-Evaporation and MEP-Transpiration models provide more reliable estimates of hourly ET than the Bowen ratio method. This is based on the modelling results from the Lignum site and the Copperburr site where data are available for both methods. The project also demonstrates that the DST radiation modelling (based on UAV-LiDAR data derived DEMs and global downwelling shortwave radiation) and distributed iButtons measurements together, provide a parsimonious approach to monitor the temporal and spatial variation of evapotranspiration from understorey and short-vegetation surfaces in the floodplain environment.

The results indicate that the River Red Gum understorey on average lost 1.2 mm per day over the observation period (September 2021-March 2022), while the Copperburr surface lost 1.7 mm per day, and the Lignum surface lost 2.0 mm per day. Based on an averaged 1.63 mm ET loss per day, it means 2.9 ML of water loss per hectare due to evapotranspiration from understorey and short vegetation surfaces in the floodplain. This may sum up to a significant component of water balance of the Murray Darling Basin.

The project has developed methodology to map floodplain ET from understorey and short-vegetation surfaces. This includes a new metnhod to map understorey surface temperature from drone observations, an adapted method to map understorey net radiation, and a site-specific relationship to map River Red Gum leaf area index. With this methodological development, the study demonstrates the reliability of using the MEP-evaporation model for producing understorey hourly and daily ET maps.

References

Gutierrez-Jurado, H., H. D. Guan, J. Wang, H. L. Wang, R. L. Bras, and C. T. Simmons (2015), Maximum Entropy Production Modeling of Evapotranspiration Partitioning on Heterogeneous Terrain and Canopy Cover: advantages and limitations., in *American Geophysical Union Fall Meeting*, edited, American Geophysical Union, San Francisco, USA.

Hajji, I., D. F. Nadeau, B. Music, F. Anctil, and J. F. Wang (2018), Application of the Maximum Entropy Production Model of Evapotranspiration over Partially Vegetated Water-Limited Land Surfaces, *J. Hydrometeorol.*, *19*(6), 989-1005, doi:10.1175/jhm-d-17-0133.1.

Heilman, J. L., C. L. Brittin, and C. M. U. Neale (1989), Fetch requirements for Bowe-ratio measurements of latent and sensible heat fluxes, *Agricultural and Forest Meteorology*, *44*(3-4), 261-273, doi:10.1016/0168-1923(89)90021-x.

Jiang, B., et al. (2015), Empirical estimation of daytime net radiation from shortwave radiation and ancillary information, *Agricultural and Forest Meteorology*, *211*, 23-36, doi:10.1016/j.agrformet.2015.05.003.

Lamaud, E., J. Ogee, Y. Brunet, and P. Berbigier (2001), Validation of eddy flux measurements above the understorey of a pine forest, *Agricultural and Forest Meteorology*, *106*(3), 187-203, doi:10.1016/s0168-1923(00)00215-x.

Liu, N., Z. J. Deng, H. L. Wang, Z. D. Luo, H. A. Gutierrez-Jurado, X. G. He, and H. D. Guan (2020), Thermal remote sensing of plant water stress in natural ecosystems, *Forest Ecology and Management*, *476*, doi:10.1016/j.foreco.2020.118433.

Liu, N., H. D. Guan, Z. D. Luo, C. C. Zhang, H. L. Wang, and X. P. Zhang (2017), Examination of a coupled supply-and demand-induced stress function for root water uptake modeling, *Hydrology Research*, *48*(1), 66-76, doi:10.2166/nh.2016.173.

Liu, W. J., H. D. Guan, H. A. Gutierrez-Jurado, E. W. Banks, X. G. He, and X. P. Zhang (2022), Modelling quasi-three-dimensional distribution of solar irradiance on complex terrain, *Environmental Modelling & Software*, *149*, doi:10.1016/j.envsoft.2021.105293.

Payero, J. O., C. M. U. Neale, J. L. Wright, and R. G. Allen (2003), Guidelines for validating Bowen ratio data, *Transactions of the Asae*, *46*(4), 1051-1060.

Tanner, B.D., Greene, J.P., Bingham, G.E., 1987. A Bowen ratio design for long term measurements, in: ASAE 1987 International Winter Meeting.

Wang, J., and R. L. Bras (2009), A model of surface heat fluxes based on the theory of maximum entropy production, *Water Resour. Res.*, *45*, 15, doi:10.1029/2009wr007900.

Wang, J. F., and R. L. Bras (2011), A model of evapotranspiration based on the theory of maximum entropy production, *Water Resour. Res.*, *47*, 10, doi:10.1029/2010wr009392.

Wang, Y., and H. L. Fang (2020), Estimation of LAI with the LiDAR Technology: A Review, *Remote Sensing*, *12*(20), doi:10.3390/rs12203457.

Yang, Y. T., H. D. Guan, J. L. Hutson, H. L. Wang, C. Ewenz, S. H. Shang, and C. T. Simmons (2013), Examination and parameterisation of the root water uptake model from stem water potential and sap flow measurements, *Hydrol. Process.*, *27*(20), 2857-2863, doi:10.1002/hyp.9406.